RELATIVE TIMING OF ALBITIZATION AND CHLORINE ENRICHMENT IN BIOTITE IN PROTEROZOIC SCHISTS, SNAKE CREEK ANTICLINE, MOUNT ISA INLIER, NORTHEASTERN AUSTRALIA

MICHAEL J. RUBENACH

School of Earth Sciences, James Cook University, Townsville, 4811, Australia

ABSTRACT

In the Snake Creek area, near Cloncurry, Mount Isa Inlier, in northeastern Australia, multiple episodes of deformation, low-pressure metamorphism, intrusion of abundant mafic and granitic bodies, and extensive metasomatism occurred throughout the Mesoproterozoic Isan Orogeny. Albitites and associated metasomatic biotite-rich schists are abundant in the core of the Snake Creek Anticline, and are concentrated in five areas. Albitization peaked during D_1 and was commonly localized along shear zones. Muscovite schists adjacent to albitites were altered to albite-bearing biotite-rich schists. Porphyroblast growth in metasomatic rocks commenced with cordierite and andalusite from late syn-D_1, but episodic growth continued to post-D_5, with the peak of metamorphism occurring late syn-D_3 to early syn-D_4. The timing of albitization was determined from the presence or absence of albite in various stages of andalusite growth, and similarly the Mg# [Mg/(Mg + Fe)] and Cl contents of biotite were examined over the span of porphyroblast-growth history. Differential mass-transport of Mg and Fe took place from the albitites to the adjacent schists predominantly during D_1, and the Mg# for biotite in metasomatic rocks was largely fixed during D_1. The Cl content of the matrix biotite varies considerably in the different areas of albitite development, from below detection to a maximum of 1.5 wt%. This could indicate that the Cl enrichment event was not related to albitization, but there is nevertheless an overall spatial relationship between them. In any particular sample, the Cl content in biotite is generally higher in the matrix than for inclusions in late andalusite, with inclusions in early andalusite being the poorest in Cl. Enrichment of Cl in biotite is a function of $f(HCl)/f(H_2O)$ rather than salinity, and so could be related to the replacement of muscovite by albite, as this involves release of H^+. The ratio $f(HCl)/f(H_2O)$ would have been low during periods of high flux of fluid that produced the albitites, but increased during low flux, in the waning stages of albitization, resulting in maximum enrichment in Cl relatively late in the metasomatic history.

Keywords: andalusite, metasomatism, albitization, biotite, Cl enrichment, Cloncurry area, Australia.

SOMMAIRE

De multiples épisodes de déformation, de métamorphisme à faible pression, d'intrusion de magmas abondants mafique et granitique, et de métasomatose répandue ont eu lieu tout au long de l'orogenèse Isanne, d'âge mésoprotérozoïque, dans la région de Snake Creek, près de Cloncurry, socle de Mount Isa, dans le nord-est de l'Australie. Les albitites et les schistes enrichis en biotite lors d'une métasomatose sont abondants au centre de l'anticlinal de Snake Creek, et sont surtout développés à cinq endroits. L'albitisation a atteint son développement maximum au cours de l'événement D_1, surtout le long de zones de cisaillement. Les schistes à muscovite voisins des albitites ont été altérés à des schistes à biotite et à albite. La croissance des porphyroblastes dans les roches métasomatiques a commencé avec la cordiérite et l'andalousite à partir du stade D_1 tardif, mais la croissance épisodique a continué au delà de D_5, le paroxysme du métamorphisme ayant lieu soit tard au cours de l'événement D_3, soit au début de l'événement D_4. Le déroulement relatif de l'albitisation dans le temps a été déterminé par la présence ou absence de l'albite aux divers stades de croissance de l'andalousite, de même qu'en fonction du rapport Mg# [Mg/(Mg + Fe)] et de la teneur en Cl de la biotite au cours de l'évolution des porphyroblastes. Un transfert différentiel de Mg et de Fe a eu lieu aux dépens des albitites en direction des schistes avoisinants, surtout au cours de D_1, et la valeur de Mg# de la biotite des roches métasomatiques a largement été fixée à cette époque. La teneur en Cl de la biotite de la matrice varie considérablement d'un des centres d'albitization à l'autre, d'inférieure au seuil de détection jusqu'à un maximum de 1.5% (poids). Cette observation pourrait indiquer que l'enrichissement en Cl n'est pas liée à l'albitisation, mais il y a néanmoins une relation globale entre ces phénomènes dans l'espace. Dans un échantillon quelconque, la teneur en Cl de la biotite de la matrice dépasse en général celle de la biotite incluse dans l'andalousite tardive, et les inclusions dans l'andalousite précoce sont les plus dépourvues en Cl. L'enrichissement de la biotite en Cl est fonction de $f(HCl)/f(H_2O)$ plutôt que de salinité, et donc pourrait être liée au remplacement de la muscovite par l'albite, qui implique la libération de H^+. Le rapport $f(HCl)/f(H_2O)$ aurait été faible durant les périodes de flux élevé de fluides impliqués dans la production des albitites, mais aurait augmenté là où le flux était plus faible aux stades tardifs de l'albitisation, avec comme résultat un enrichissement maximum en Cl relativement tard dans l'évolution métasomatique.

(Traduit par la Rédaction)

Mots-clés: andalousite, métasomatose, albitisation, biotite, enrichissement en Cl, région de Cloncurry, Australie.

e-mail address: michael.rubenach@jcu.edu.au

INTRODUCTION

Studies of porphyroblast–matrix relationships have contributed significantly to our understanding of metamorphic processes and to the relative timing of thermal and structural events. A comparison of patterns of inclusion trails in porphyroblasts with matrix foliations indicates not only the timing of metamorphic events relative to deformation history (Zwart 1960, Vernon 1978), but also the sequential timing with respect to the development of a crenulation cleavage during a specific deformation event (Bell & Rubenach 1983, Reinhardt & Rubenach 1989). Metamorphic microstructures may also reveal information about reaction processes in metamorphic rocks. In a landmark study, Dugald Carmichael (1969) convincingly argued that reactions in schists commonly proceed *via* complex pathways, involving matrix minerals in a catalytic capacity (in addition to their role as reactants or products), with coupled ionic diffusion through intergranular fluids between sites of dissolution and growth. Prior to Carmichael's study, no adequate explanations existed for the development of textures around porphyroblasts in schists due to a prograde reaction.

In previous studies of schists from the Snake Creek Anticline, Rubenach & Barker (1998) and Rubenach & Lewthwaite (2002) documented the common occurrence of albitites (as veins, as a replacement of metapsammitic rocks, and along shear zones). They also used the presence or absence of albite inclusions in porphyroblasts of andalusite, staurolite, garnet and cordierite to argue that albitization has been the result of synmetamorphic metasomatism, as opposed to concentration of Na during diagenetic processes in the sedimentary protoliths. Thus inclusion trails in porphyroblasts were found to be instrumental in placing metasomatic events within a P–T–t (pressure – temperature – time) path. Rubenach & Lewthwaite (2002) further proposed that biotite alteration of schists adjacent to albitites was related to albitization. Routine electron-microprobe analyses indicate that biotite grains in the metasomatic rocks are commonly enriched in chlorine, and that such enrichment defines complex patterns in space and time. In this paper, I describe the spatial distribution of chlorine enrichment in biotite, and compare the composition of matrix biotite with that of biotite included in various growth-zones within andalusite porphyroblasts. Combining biotite composition with microstructural development allowed investigation of the relative timing of albitization and Cl enrichment in biotite, and led to a test whether or not the two processes are genetically related. Although albitization may be linked to infiltration of saline fluids (Oliver *et al.* 1993, Williams *et al.* 1999), experimental and thermodynamic studies indicate that chlorine enrichment in biotite is a function of HCl activity rather than salinity (Munoz & Swenson 1981, Zhu & Sverjensky 1991). There is, therefore, no necessary link between Cl enrichment in biotite and albitization.

GEOLOGY OF THE SNAKE CREEK ANTICLINE

The Snake Creek area is situated about 20 km south of Cloncurry on the Roxmere cattle property, and is accessed along the western side by tracks. The region has low annual rainfall and sparse vegetation that includes spinifex grass. Numerous ephemeral streams and low hills provide localized good exposure.

The study area forms part of the Eastern Fold Belt of the Proterozoic Mount Isa Inlier (Figs.1, 2). Sedimentation occurred in intracontinental rift basins that have been grouped into three cover sequences (Blake & Stewart 1992). Rocks in the Snake Creek area consist of the Corella beds (cover sequence 2, depositional age 1760–1725 Ma), which are in tectonic contact with the Soldiers Cap Group (cover sequence 3, depositional ages 1712–1654 Ma) (Page & Sun 1998). The Corella beds are mainly scapolite-bearing calc-silicate rocks that have been extensively brecciated and hydrothermally altered. The Soldiers Cap Group consists of a lower unit of rhythmically bedded metapsammite and schist (Llewellyn Creek Formation), formed by metamorphism of turbidites, overlain by a unit of schist, metapsammite, quartzite and amphibolite (the Mount Norna Quartzite). A sill complex of gabbro, dolerite and tonalite intruded near the top of the Llewellyn Creek Formation prior to deformation, the mafic rocks being largely converted to amphibolite.

Deformation and metamorphism of the Snake Creek area occurred episodically during the Isan Orogeny, which extended from 1610 to 1500 Ma. Intrusion of mainly granitic magmas that led to the Williams and Naraku batholiths (1547–1500 Ma) overlapped with the latter half of the Isan Orogeny (Page & Sun 1998). Low-pressure and high-temperature metamorphism is recorded by multiple events of porphyroblast growth. Metamorphic zones for the Snake Creek Anticline (Fig. 2) are composite, wherein andalusite, garnet, staurolite, kyanite and sillimanite exhibit multiple growth (Table 1). The sillimanite – K-feldspar zone is related to the relatively late 1520–1536 Ma Saxby Granite, one of units of the Williams Batholith.

The structural evolution of the Snake Creek area used in this paper is after Rubenach & Lewthwaite (2002), who recognized five major events. The first three were associated with penetrative strain (D_1, D_2, D_3) whereas the effects of D_4 and D_5 were more localized. The first two events probably resulted from generally north–south compression. Event D_1 produced folds with shallowly dipping axial planes and east-northeasterly-trending fold axes (Loosveld 1989), whereas D_2 resulted in upright east–west folds (Rubenach & Lewthwaite 2002). Folds and matrix foliations produced in the D_1 and D_2 events are only locally preserved, but
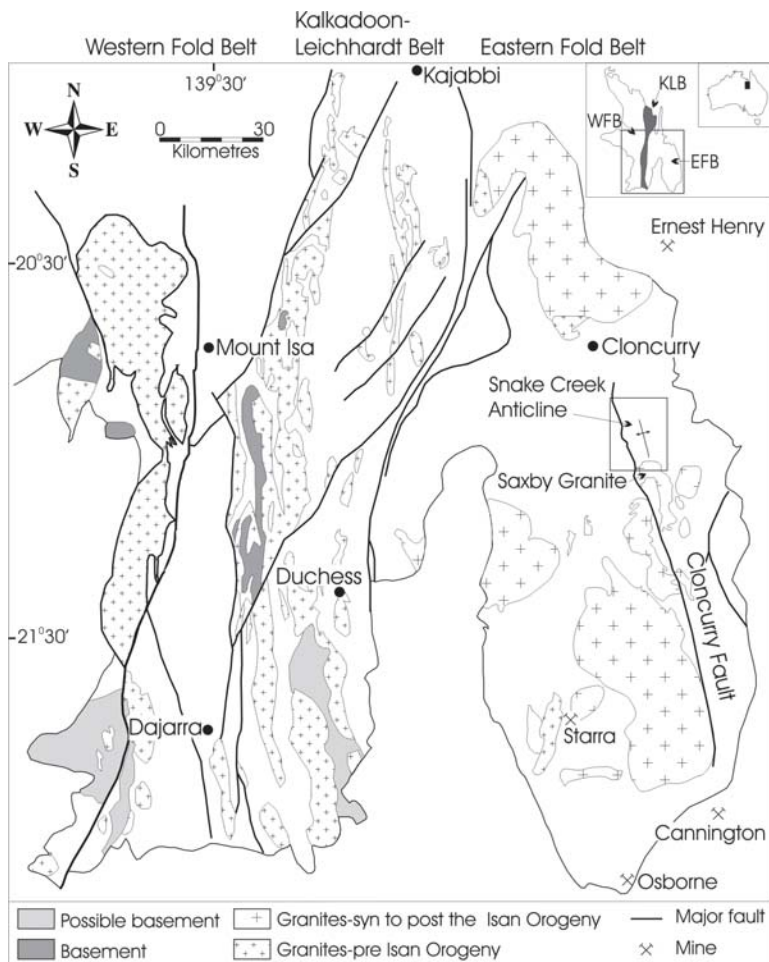
FIG. 1.   Map of the Mount Isa Inlier, showing the location of the Snake Creek Anticline south of Cloncurry, in the Eastern Fold Belt.

S_1 and S_2 are well preserved as trails of inclusions in porphyroblasts (Rubenach & Lewthwaite 2002). The D_3 event resulted from east–west compression, which produced folds and the dominant steeply dipping north–south foliation in the Eastern Fold Belt. The Snake Creek Anticline is interpreted as an F_3 fold, the southern part of which is an antiformal syncline because of interference with a recumbent F_1 fold. The D_3 event (Rubenach & Lewthwaite 2002, this paper) is referred to as D_2 in other publications (*e.g.,* Rubenach & Barker 1998, Oliver *et al.*, in press). Event D_4 resulted in crenulations and rare mesoscopic folds with shallowly dipping axial planes. The effects of D_4 are mainly observed in the Mount Norna Quartzite, in the western part of the area, as are the steep north-northwesterly-trending crenulations produced in the D_5 event. The peak of

metamorphism, represented by the growth of sillimanite, occurred somewhere between late D_3 and early D_4 on the basis of microstructures, but andalusite growth can be related to each of the above five events (Rubenach & Lewthwaite 2002). Note that the isograds sharply cut the stratigraphy in the west and northwest of the area (Fig. 2), and the apparent folding of isograds by the Snake Creek Anticline is possibly due to its reactivation during D_5. On the basis of pseudosections and phase diagrams determined using THERMOCALC for assemblages in the systems KFMASH and NASH, conditions of metamorphism for the sillimanite isograd were found to be around 580 C and 400 MPa (M.J. Rubenach, unpubl. data). Earlier, some investigators (*e.g.,* Rubenach & Barker 1998, Rubenach & Lewthwaite 2002) suggested that the peak of metamorphism in the
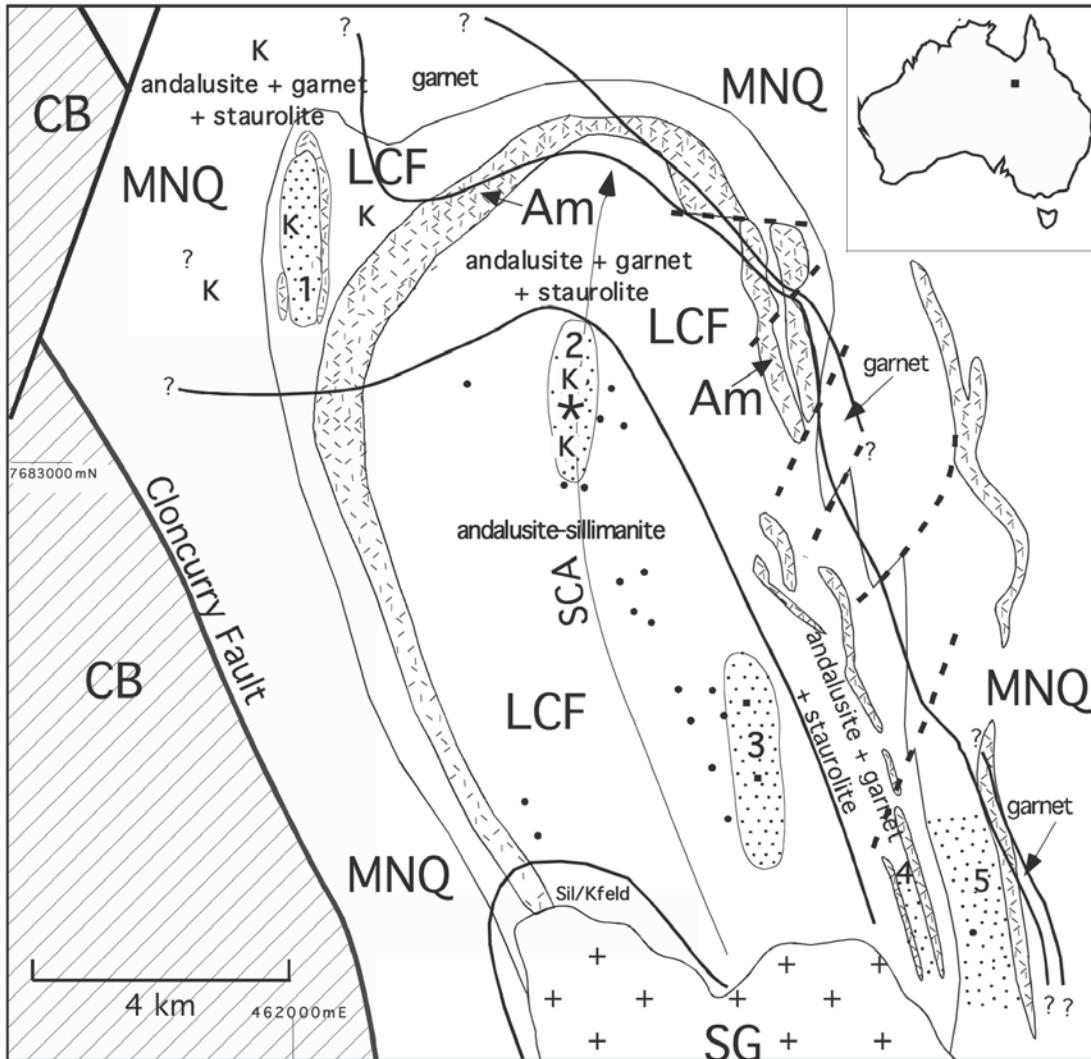
FIG. 2.   Map of the Snake Creek area, modified from Rubenach & Lewthwaite (2002). Geological units are as follows: CB: Corella beds, LCF: Llewellyn Creek Formation, MNQ: Mount Norna Quartzite, SG: Saxby Granite, and AM: amphibolite. Metamorphic zones and isograds are shown, along with kyanite localities (K), cordierite localities (filled circles), and the axial trace of the Snake Creek Anticline (SCA). Definite faults are shown as heavy lines, and possible faults as heavy dashed lines. Areas of intense albitization are designated 1–5, but albitite occur throughout the Lewellyn Creek Formation. Cordierite occurrences are closely associated with local albitite. Locality 430 in area 2 is shown as a star.

Eastern Fold Belt took place at *ca*. 1540 Ma because of the occurrence of foliated granites with igneous ages of 1545–1547 Ma. However, recent U–Pb dates of mona-zite, zircon, and titanite indicate metamorphic ages of 1580–1600 Ma (Giles & Nutman 2002, Gautier *et al*. 2001, Rubenach *et al*. 2001), consistent with an earlier U–Pb SHRIMP date of 1584 Ma for a zircon rim in a gneiss (Page & Sun 1998). I now believe that the folia-

tions in the 1545–1547 Ma granites formed in localized shear-zones that postdated the peak of metamorphism.

Low-pressure metamorphism, in part recorded by episodic growth of andalusite, occurred throughout the Mount Isa Inlier. The intrusion of magmas made the most significant contribution to thermal perturbations in the middle crust during the Isan Orogeny (Foster & Rubenach 2001). In the Snake Creek area, a north–

south-striking swarm of basalt dykes intruded during D_3, with numerous dykes parallel to S_3 and possessing S_3 foliations. Syn-D_3 pegmatite sheets are fairly common in the sillimanite zone. In the south of the area, a composite body of Saxby Granite consists of monzogranite, granite and subordinate basaltic rocks. To the south of the area, other bodies of Saxby Granite have provided SHRIMP U–Pb (zircon) ages between 1536 ∠ 12 and 1520 ∠ 8 Ma. Mark *et al.* (1999) suggested that D_5 was *ca.*1527 Ma on the basis of SHRIMP dating of two granites, one foliated and the other unfoliated. The western half of Saxby Granite in the Snake Creek area shows abundant evidence of magma mingling and mixing of granitic and mafic rocks, and an aureole of sillimanite – K-feldspar gneisses up to 1 km wide (Fig. 2). The metamorphism of these gneisses was previously interpreted as syn-D_3 (Rubenach & Lewthwaite 2002). In contrast, the aureole surrounding the eastern half of the Saxby Granite, where there are no mingled mafic rocks, is typically only meters wide, with the development of intrusion-related andalusite and sillimanite in muscovite schists. The higher-temperature aureole is likely to be related to the higher proportion of mafic rocks in the western half of the Saxby Granite body.

The Cloncurry Fault is interpreted as dipping about 35 to the east on the basis of a seismic traverse situated just north of the study area (Goleby *et al.* 1996). Thus the Soldiers Cap Group structurally overlies the older Corella beds, implying that the main movement on the fault was extensional. However, reactivation of the fault as a post-D_3 thrust is highly likely, as sillimanite-zone Soldiers Cap rocks have been juxtaposed against greenschist-facies rocks of the Corella beds. Abundant small bodies of granite and gabbro have been emplaced along the Cloncurry Fault, and are associated with extensive development of calc-silicate breccias, with al-

teration assemblages including combinations of calcite, albite, K-feldspar, pyroxenes (diopside–hedenbergite, aegirine-augite), amphiboles (actinolite, ferrohastingsite, magnesioriebeckite), magnetite, and hematite.

The Eastern Fold Belt is noted for the widespread occurrence of Fe-oxide – Cu – Au and Pb–Zn–Ag mineralization (Williams 1998). Most of the deposits have at least some associated albitites, and the Osborne Cu–Au deposit is hosted in a thick package of albitized gneisses (Adshead *et al.* 1998). Albitites, pegmatites and mineralization at the Osborne mine have been dated at *ca.* 1595 Ma (Gautier *et al.* 2001, Rubenach *et al.* 2001). However, U–Pb dating of titanite from calc-silicate-hosted albitites elsewhere in the Eastern Fold Belt have yielded ages of 1521–1555 Ma, a range overlapping with the emplacement of the Williams–Naraku batholiths and the formation of the Eloise and Ernest Henry Cu–Au deposits (Oliver *et al.*, in press).

In conclusion, intrusions of granitic magma, low-pressure metamorphism, extensive metasomatism (notably albitization) and Cu–Au mineralization occurred periodically throughout the 1500–1610 Ma Isan Orogeny.

ALBITITES AND BIOTITE-RICH SCHISTS

Details of the mineral assemblages and development of albitites and related biotite-rich schists are given in Rubenach & Barker (1998) and Rubenach & Lewthwaite (2002). Albitites are abundant throughout the Llewellyn Creek Formation, less so in the Mount Norna Quartzite, but are concentrated in five areas (Fig. 2). Albitites occur in three settings: (1) as replacement of pelitic schists and metapsammitic rocks along D_1 shear zones (up to several meters wide), (2) as selective replacements of muscovite-bearing metapsammite beds near shear zones, and (3) as infill veins of thickness less than 1 cm. They are comprised of fine-grained granular albite, accessory rutile or ilmenite, with or without quartz and biotite, and locally contain garnet, staurolite, cordierite, andalusite, kyanite, sillimanite and gedrite. Albite compositions are in the range An_{0-7}, with compositions of An_{2-3} being most common. Staurolite and garnet are more common in areas 1, 4 and 5, whereas cordierite is quite abundant in areas 2 and 3, and is also strongly associated with minor occurrences of albite throughout the core of the Snake Creek Anticline (Fig. 2). Garnet and cordierite are mutually exclusive. Albitites that have replaced pelitic rocks commonly contain more than 90% albite with little to no quartz, whereas albitized metapsammites contain 20–80% quartz. Biotite-rich schists typically occur adjacent to shear zones, and range in width from less than 1 meter to tens of meters (Figs. 3, 4). They are generally quartz-bearing, free of muscovite, and consist of similar assemblages to the albitites, but with albite generally less than 20% and biotite over 40%. Contacts between replacement albitites and biotite-rich schists are generally quite

TABLE 1. CHART SUMMARIZING THE TIMING OF ALBITIZATION, CHLORINE ENRICHMENT, AND PORPHYROBLAST GROWTH UP TO THE END OF D_5, SNAKE CREEK ANTICLINE, MOUNT ISA INLIER, AUSTRALIA

	D_1	D_2	D_3	D_4	D_5
cordierite	—				
garnet	—	—	—	—	—
staurolite		—	—	—	—
andalusite	?	—	—	—	—
kyanite		—			—
sillimanite			—	—	
albite	—	?	—	?	—
Cl enrichment	—	?	—	?	—

The heavier lines denote periods of more intense albitization (episode D_1) and Cl enrichment (episode D_3).
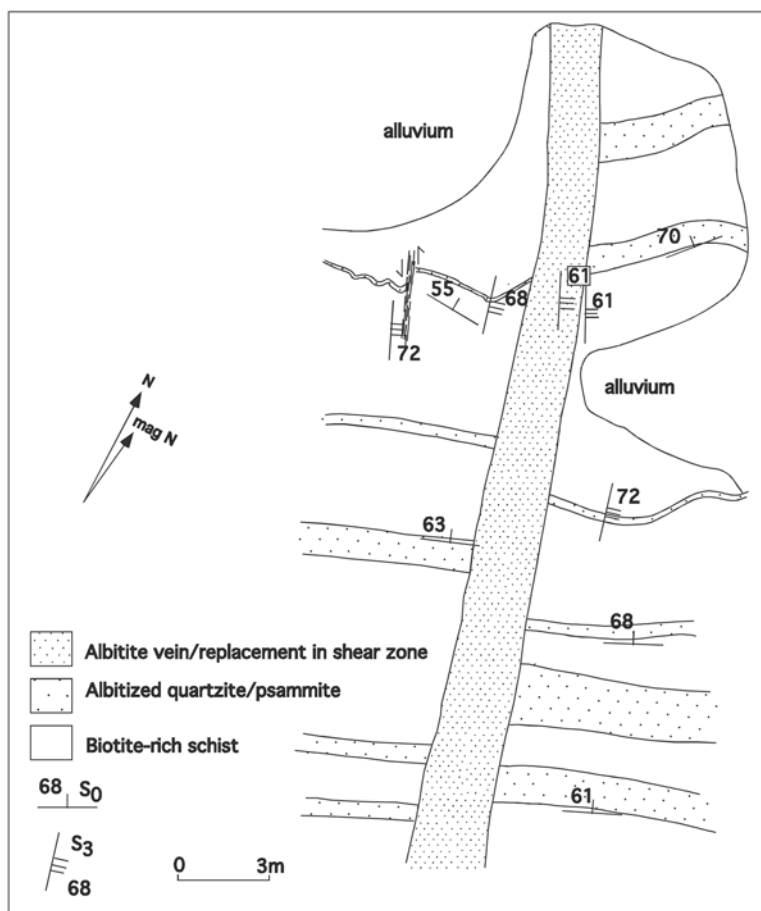
Fig. 3. Map of the location 430, area 2, modified from Rubenach & Lewthwaite (2002). The central albitite occupies a shear zone in the hinge of a F_3 fold, and consists of fine-grained albite with minor biotite and localized cordierite replaced by albite and biotite. The biotite-rich schists are metasomatized and pelitic to semipelitic in composition, and consist of biotite, quartz, replaced cordierite, andalusite, albite and localized muscovite. Thin lenticular veins of albite occur in schists and are parallel to the main vein.

sharp, whereas contacts between the biotite-rich schists and the muscovite-bearing schists and metapsammitic rocks that they replaced are either sharp or gradational.

Extensive post-D_3 albitization also occurs in association with breccias in the Corella beds, and in the Mount Norna Quartzite adjacent to the Cloncurry Fault (de Jong & Williams 1995, Oliver *et al.*, in press), but is not considered in this study.

Timing of albitization

Rubenach & Lewthwaite (2002) proposed that the albitization that produced the majority of the albitites and biotite-rich schists was syn-D_3, partly on the basis

of occurrences of steeply dipping albitite in shear zones of north–south orientation, such as location 430 shown in Figure 3. However, a recent discovery in area 3 of albite veins and alteration oriented parallel to the axial planes of F_1 recumbent folds strongly suggests the presence of some syn-D_1 albitization. This is supported by thin-section studies indicating that the coarser infill of veins has been recrystallized to finer-grained albite in zones parallel to S_1 (Fig. 5), and biotite grains in the adjacent biotite-rich schist are clearly oriented in both the S_1 and S_3 directions.

Whereas away from zones of albitization, "unmetasomatized" andalusite schists commonly contain garnet, cordierite is typically associated with albitization. This
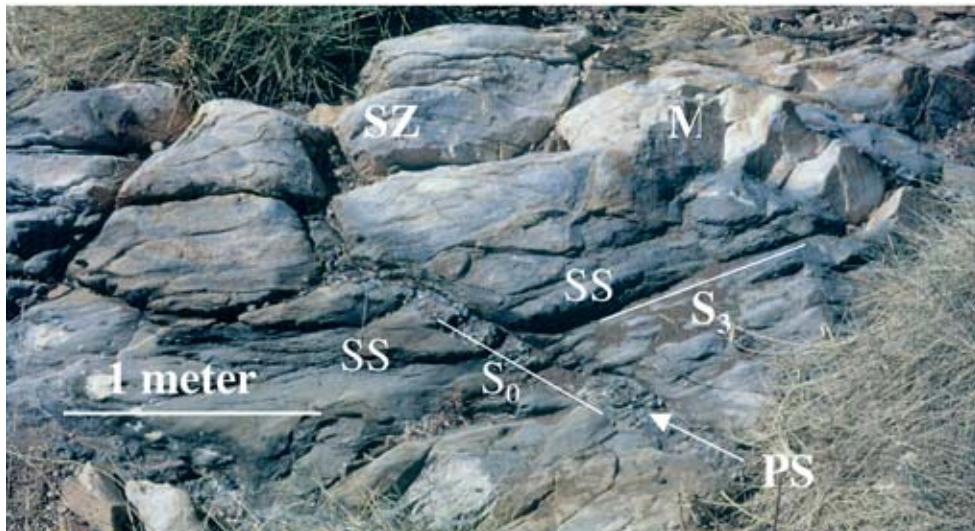
FIG. 4.   Field photograph showing a body of albitite in a shear zone (SZ), a layer of albitized metapsammite (M), layers of pelitic schist (PS) and layers of semischist (SS). The pelitic and semischist layers consist of biotite, quartz and albite, with abundant andalusite and replaced cordierite in the pelitic layer. Bedding is transected by the foliation (S_3) at a high angle. The location is in area 2, a few hundred meters north of location 430.
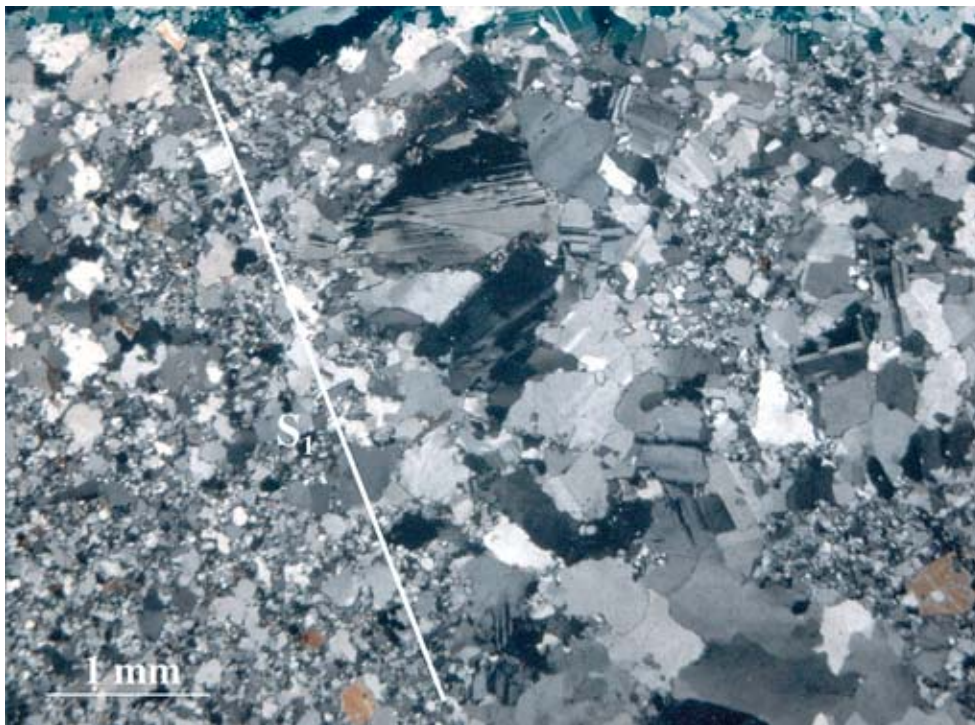

FIG. 5.   Photomicrograph of a deformed vein of albitite. Coarser grains of albite are relics from a vein, with the rest of the vein having been recrystallized to finer-grained aggregates during D_1. The orientation of S_1 is indicated. Elsewhere in this thin section, albite–biotite schist shows biotite in both the S_1 and S_3 orientations. Crossed nicols.

can be explained by differential movement of Mg, Fe and Mn during metasomatism, which led to an increase in Mg# [*i.e.,* Mg/(Mg + Fe)] in schists, favoring cordierite growth over garnet (M.J. Rubenach, unpubl. data). Most cordierite has reacted to form andalusite according to the reaction:

$$Crd + Ms + Qtz = And + Bt$$

Relict porphyroblasts of cordierite are only preserved in situations where they were protected from reaction with muscovite, such as in a few cores of andalusite, and in some muscovite-free albite-rich rocks, where they are rimmed by biotite and andalusite or, less commonly, staurolite, kyanite and sillimanite. Most cordierite has been replaced by various combinations biotite, albite, quartz, andalusite and tourmaline. Catalytic processes and coupled ionic diffusion between sites of dissolution and growth were likely to be involved in the replacement of cordierite, according to the model first presented by Carmichael (1969) for kyanite–sillimanite reactions. Cordierite has been generally replaced by biotite and quartz, with or without albite and tourmaline, whereas andalusite replaced matrix muscovite, quartz, biotite and albite. Direct replacement of cordierite by andalusite occurred only where the relatively larger porphyroblasts of andalusite enveloped cordierite already partly replaced by biotite. Potassium, Mg, Fe, Si and possibly Al were exchanged between sites of cordierite replacement and andalusite growth.

Evidence was presented in Rubenach & Lewthwaite (2002, their Fig. 6a) that at least some cordierite overgrew S_2, either late in D_2 or early in D_3. However, additional oriented samples used in this study have revealed the presence of some cordierite porphyroblasts with inclusions that are either not obviously oriented or define a weak S_1 foliation. Inclusions of albite occur in these cordierite porphyroblasts, providing additional support for the syn-D_1 occurrence of albitization. Andalusite porphyroblasts in samples from areas 2 and 3 commonly exhibit several stages of growth. Inclusions of quartz and biotite in stage-1 and stage-2 andalusite are typically relatively fine-grained, whereas inclusions in stage-3 andalusite are coarser, generally of similar grain-size and orientation as grains in the adjacent matrix. Stage-1 andalusite, by far the most abundant, either lacks trails of inclusions or shows trails that define a weak shallowly dipping S_1 foliation (Fig. 6). In the latter case, andalusite is interpreted as growing in the late syn-D_1 to early syn-D_2 period. Replaced porphyroblasts of cordierite are commonly included in stage-1 andalusite, indicating that such cordierite grew prior to, or possibly overlapping with, stage-1 andalusite. Stage 2 is only rarely developed, and consists of andalusite that has overgrown a relatively fine-grained foliation (S_1) that has in places has been folded by open microfolds, possibly F_2 (Figs. 7, 8). Stage-3 andalusite is fairly common, but occurs as a quite narrow overgrowth on earlier andalusite, in some samples truncating foliations preserved in stage 1 or 2 (Fig. 6). In some rocks, stage-3 andalusite also occurs as elongate grains extending parallel to the axial traces of F_3 microfolds. Stage-3 andalusite probably grew at some point in the late syn-D_3 to early syn-D_4 period.

The above structural and microstructural observations, mainly from areas 2 and 3, indicate that albitization commenced during D_1. However, in other samples, albite is abundant in the matrix, but lacking in porphyroblasts with S_2 inclusion trails, suggesting that some albitization also occurred during D_3 (Rubenach & Lewthwaite 2002, Fig. 6c). In addition, Rubenach & Barker (1998) documented planar veins of albite cutting S_3, suggestive of late syn- to post-D_3 emplacement. In sample 430.4, all three stages of andalusite contain albite inclusions, but they are subordinate to quartz (Fig. 8). However, the immediately adjacent matrix locally contains abundant albite that transects the folded S_1 foliation and has replaced quartz, suggesting that most albite in this sample formed late syn- to post-D_3. The albite thus seems to have formed over a protracted period from syn-D_1 to post-D_3, although albitites that formed syn-D_1 are probably the most abundant. Given the structural controls, albitization was probably episodic rather than continuous. Table 1 provides a summary of the timing of metamorphism and metasomatism, and include data on the timing of Cl enrichment in biotite, as discussed below.

Another problem in timing requiring consideration is the north–south orientation of albitite-replaced shear zones in areas 1–3, particularly those in the hinges of F_3 folds. These shear zones were interpreted as forming in D_3 rather than the D_1 or D_2 events, both of which produced east–west structures (Rubenach & Lewthwaite 2002). However, andalusite containing albite along with straight S_1 trails of inclusions occurs in schists immediately adjacent to the shear zones, suggesting that albitization had commenced prior to D_3. The occurrence adjacent to north–south shear zones of relict S_1 and S_2 at some localities precludes the possibility that the shear zones represent rotated D_1 or D_2 structures. The shear zones possibly represent north–south accommodation structures separating areas of different D_1-related strain, as F_1 mesoscopic folds are more common in the eastern half of the Snake Creek Anticline. If so, the shear zones were certainly reactivated during D_3.

Biotite Compositions

In this section, I consider the chlorine content and Mg/(Mg+Fe) proportion in biotite from Snake Creek, and contrast (nonmetasomatic) muscovite schists with albitites and associated biotite-rich metasomatic schists (Table 2). Routine electron-microprobe analyses of biotite revealed significantly high Cl contents in many samples, in particular those from biotite-rich schists. The variation in biotite compositions within different

stages of growth of andalusite was documented, and possible relationships between albitization and Cl enrichment were examined. Fluorine was not detected. Biotite grains commonly occur as inclusions in andalusite porphyroblasts that may have protected them from subsequent reactions in the matrix and from interaction with any later-stage infiltrating fluids. Thus each event of andalusite growth potentially preserves the composition of biotite that existed at that particular stage.

It has been demonstrated that Cl in biotite is a function of HCl in fluids, not simply NaCl or other chlorides in solution (*e.g.,* Munoz & Swenson 1981). A revised expression for Cl–OH in biotite (Munoz 1992), based on the thermodynamic data of Zhu & Sverjensky (1991) and of Munoz (1992), is as follows:

$$\log f(H_2O)/f(HCl) = 1000/T\ (1.15 - 0.55X_{Mg})$$
$$+ 0.68 - \log (X_{Cl}/X_{OH}),$$

where X_{Mg} is Mg/(sum of octahedrally coordinated cations), and X_{Cl} is the mole fraction of Cl in the hydroxyl site. As well as the $f(H_2O)/f(HCl)$ ratio, the maximum amount of Cl that can be incorporated in biotite depends on X_{Mg} (Mg#), owing to Mg–Cl avoidance (Munoz 1984, Oliver *et al.* 1992).

Figure 9 shows Mg# *versus* chlorine contents of matrix biotite and biotite inclusions in andalusite for unmetasomatized muscovite schists, metasomatic biotite-rich schists, and albitites. In Tables 3 and 4, I summarize biotite compositions in the various lithologies and areas of albitization, respectively. Compositions range from annite to Fe-rich phlogopite, with incorporation of the more aluminous siderophyllite end-member being less than 30%. The "chlorine saturation line" indicates the maximum measured chlorine content of biotite at Snake Creek; given the negative slope of the line, this parameter is clearly a function of Mg#, reflecting Mg–Cl avoidance. However, matrix biotite compositions that plot along the "maximum Cl line" gave values of log $(f(H_2O)/f(HCl))$ in the range 3.0 to 4.0 [calculated at 580 C, according to Munoz (1992)]. This finding suggests an order-of-magnitude difference in $f(H_2O)/f(HCl)$ for fluids with relatively high HCl contents. Important observations and conclusions that can be drawn from biotite compositions (Figs. 9–10 and Tables 3 and 4) are summarized below:

1. Although there is overlap, the Mg# values of biotite in many biotite-rich schists, especially in area 2, are higher than those in unmetasomatized muscovite schists, the exceptions being some biotite-rich schists containing garnet or staurolite (or both). The differences in Mg# are interpreted as being the result of differential movement of Mg and Fe during albitization and formation of the biotite-rich schists (see Discussion).

2. The Cl content of biotite in any particular sample of biotite-rich schist generally increases in the order early andalusite (mainly pre-D_3), late andalusite (late syn- to post-D_3) to matrix. In a few samples, however, biotite in inclusions in late andalusite has a higher Cl than that in the matrix. The corresponding values of Mg# do not show a significant change, suggesting that Mg# was essentially set early in the metasomatic history.

3. The Cl contents of biotite in the matrix and present as inclusions in late andalusite in biotite-rich schists vary, with each area showing a distinct range (Table 4). In area 1, Cl contents are below detection in all samples. In area 2, they all lie close to the "chlorine saturation line". In areas 3–5, they are below the saturation line, and in some samples are below the detection limits.

4. In all areas, the Cl content of biotite in albitites is, with a few exceptions, below the saturation line, and some samples, including a few from area 2, are below detection limits.

Figure 10 shows Mg# and wt% Cl contents of biotite in the matrix of albitites and biotite-rich schists from location 430 (Fig. 3), plotted against distance from the main vein. Biotite grains in albitites have Mg# value similar to those in immediately adjacent biotite-rich schists. There is a general decrease in Mg# away from the main vein, except for high values in two samples collected over four meters away from the main vein. Most biotite-rich schists have a higher Mg# than unmetasomatized muscovite schists, reflecting the differential movement of Fe and Mg during alteration (see Discussion).

Figure 11 shows Mg# and Cl values for a single sample (430.4) of schist that has large porphyroblasts of andalusite and that shows a strong S_1 foliation overprinted by F_3 folds and an S_3 crenulation cleavage (Figs. 7, 8). Particular layers were selectively metasomatized to albite or biotite–albite schist, with some layers preserved as unaltered muscovite – quartz – biotite schist. Most of the andalusite in the sample belongs to stage 1, and has overgrown a weak shallowly dipping S_1 foliation. Stage 2 has overgrown a microfold, possibly F_2, and stage 3 is a narrow rim that preserves a strong S_1 foliation and an F_3 microfold (Fig. 8). The fact that S_1 is weak in stage 1 but very strong in the matrix and in stage-3 andalusite implies that S_1 was reactivated and intensified prior to the development of the F_3 microfold (Bell 1986). Significant variations were found in the composition of biotite in this sample. No obvious differences were found in matrix biotite in the muscovite-rich and biotite-rich layers in the schist. The matrix values show a trend close to the maximum Cl line, the lowest values of Cl occurring immediately adjacent to andalusite. Biotite inclusions in stage-1 andalusite show a trend that is at a high angle to the maximum Cl line, with very little overlap with matrix biotite. Stage-3 biotite inclusions are similar in composition to the highest-Cl and lowest-Mg# matrix biotite, whereas stage-2 biotite extends from the low-Cl and low-Mg# value of stage-3 biotite. Note that sample 430.4 covers the entire
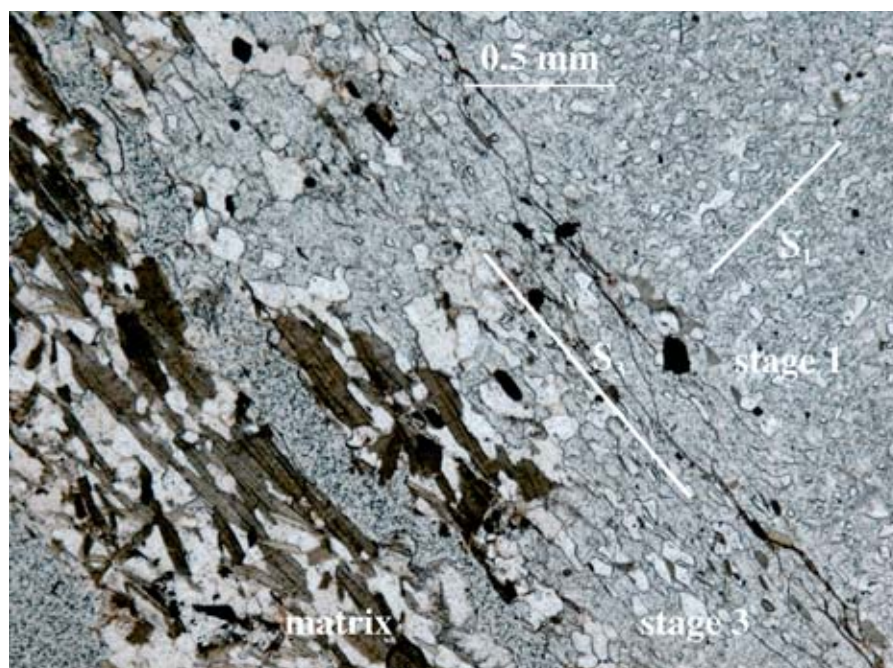
FIG. 6.   Photomicrograph of part of a large porphyroblast of andalusite, most of which belongs to stage 1, with quartz and biotite inclusions that are weakly aligned in S_1. Stage-1 andalusite probably grew sometime in the period late syn-D_1 to syn-D_2. A narrow rim of stage-3 andalusite shows a strong S_3 foliation defined by elongate grains of quartz and biotite, and probably grew in the period late syn-D_3 to syn-D_4. The matrix is biotite-rich schist composed of biotite, quartz and albite. Albite does not commonly form inclusions in the andalusite, but is abundant in replaced cordierite. Oriented sample 115 of Sayab Mohammad, location 430. Plane-polarized light.
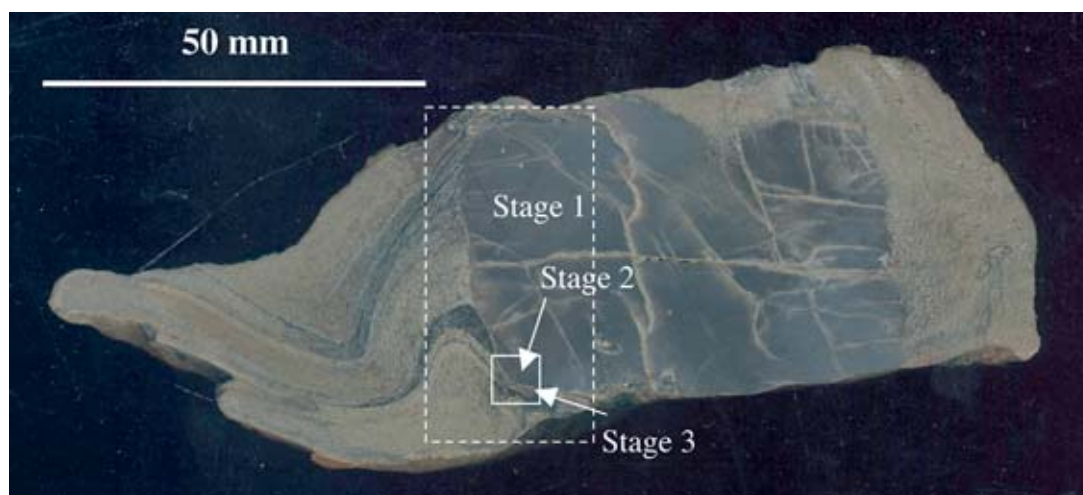
FIG. 7.   Andalusite porphyroblast in schist, sample 430.4. Relict bedding (S_0) has been folded during D_3 and is cut by an S_3 crenulation cleavage. S_1 transects S_0 at a shallow angle. Some layers have been preferentially replaced by biotite and albite, but others remain as muscovite – quartz – biotite schist. Stages 1, 2 and 3 of andalusite growth are indicated. Note the prominent dark biotite-rich layer showing an F_3 fold. A weak S_1 is preserved as trails of inclusions in stage-1 andalusite (compared with the strong S_1 in the matrix). The dashed area is the location of a polished thin section used for analysis of biotite from the matrix and from each stage of andalusite. The results are plotted on Figure 11. The small box shows the location of Figure 8.
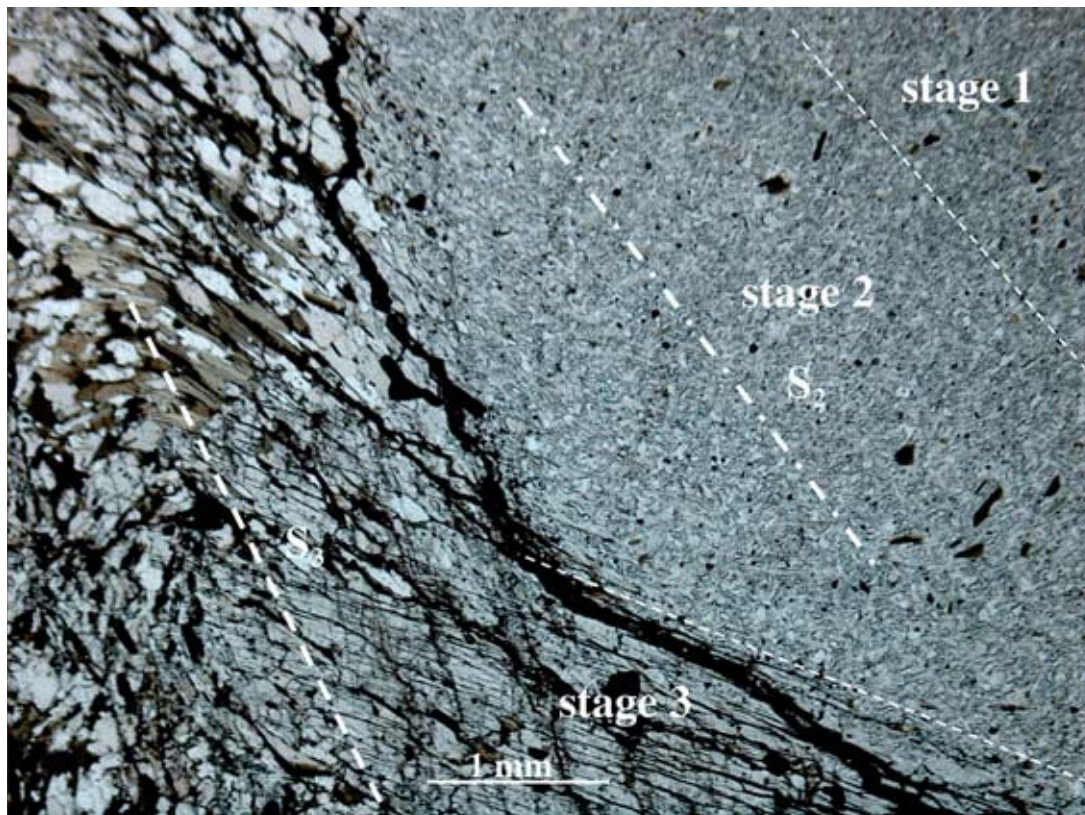
FIG. 8. Photomicrograph of specimen 430.4, showing three stages of andalusite, each of which contains inclusions of quartz, biotite and rare albite. Stage-3 andalusite and the adjacent matrix preserve an F_3 microfold, the axial trace of which is indicated. Inclusions in andalusite of stages 1 and 2 are relatively fine-grained and poor in biotite, contrasting with stage-3 inclusions and the matrix. The microfold preserved in stage-2 andalusite is possibly F_2, and the axial trace is labeled. Grain coarsening and intensification of the S_1 foliation occurred between the growth of stages 2 and 3, suggesting reactivation of S_1 prior to the development of the F_3 microfold (see text). Plane-polarized light.

Cl range of all samples analyzed, whereas the range of Mg# (0.35–0.45) is restricted to the low values in Figure 9.

DISCUSSION

Rubenach & Lewthwaite (2002) had earlier suggested that the widespread albitization in the Snake Creek Anticline commenced early in D_3, mainly on the basis of shear zones of north–south orientation developed in albitite and the observation that in some albitites, porphyroblasts with S_2 trails lack albite inclusions. Other porphyroblasts contain albite inclusions with or without S_1 or S_2 trails, but the occurrence of S_1 or S_2 trails does not preclude porphyroblast growth in a subsequent event, *i.e.*, D_3 in the Snake Creek Anticline (*e.g.*, Bell & Hayward 1991). New observations presented in

this study, especially the occurrence of albitite showing S_1 and occurring subparallel to the axial planes of F_1 folds, indicate that albitization commenced during D_1. Combined with the evidence for syn-D_3 albitization (Rubenach & Lewthwaite 2002) and the occurrence of post-S_3 albitite veins (Rubenach & Barker 1998), it is now clear that albitization extended from D_1 to post-D_3, with syn-D_1 albitites probably being the most abundant.

Figure 12 shows a model intended to explain the relationship between albitites and adjacent metasomatic biotite-rich schists. Both Fe and Mg were removed from shear zones during the more extreme albitization, and deposited, along with variable amounts of Na, to make biotite and albite in the adjacent rocks. Potassium was removed from both albitites and biotite-rich schists (Oliver *et al.*, in press, M.J. Rubenach, unpubl. data). The values of Mg# in biotite in albitites and biotite-rich

schists are mainly higher than those in unmetasomatized muscovite schists, suggesting differential migration of Mg and Fe during alteration (Table 3, Figs. 9–10). It is also possible that some Fe, along with K, was removed from the system. The fact the Mg# values for biotite occurring as inclusions in andalusite do not differ from that in the corresponding matrix by more than 0.1 suggests that most of the Fe and Mg movement occurred early in the history, probably during D_1. However, a detailed study of sample 430.4 suggests that minor differential movement of Mg and Fe continued during and after D_3 (Fig. 11).

In contrast to albitization and Mg–Fe mass transport, maximum Cl enrichment in biotite occurred late in the alteration history, probably during D_3. Such a decoupling of peak albitization and Cl enrichment could be interpreted in terms of two unrelated metasomatic events. The large variation in degree of Cl enrichment shown by biotite in the different areas of albitization, ranging from below detection in all samples in area 1 to near-saturation for matrix biotite in most biotite-rich schists in area 2, appears to support the notion of unrelated metasomatic events. Chlorine enrichment in biotite depends on the HCl content of fluid, such that infiltration of NaCl-rich fluids could produce albitization but

not Cl enrichment unless $f(HCl)/f(H_2O)$ also was sufficiently high in the brines (Munoz & Swenson 1981).

Pegmatites generated by anatexis of the Soldiers Cap Group are a possible source of acidic fluids, as associated sillimanite is quite abundant in the higher-grade rocks around the Cannington and Osborne mines at the southern extremity of the Eastern Fold Belt (Mark *et al.* 1998, Rubenach *et al.* 2001). Such sillimanite is commonly associated with S-type granite, those formed at the expense of metasedimentary protoliths, and most probably formed by base-ion leaching by acidic fluids (Vernon 1979, McLellan *et al.* 2002). However, the Cl content of biotite accompanying sillimanite at the Osborne mine is low (Adshead 1995, M.J. Rubenach, unpubl. data), so it is by no means certain that fluids derived from crystallizing pegmatites below the Snake Creek Anticline supplied the HCl-bearing fluids for Cl enrichment in biotite.

Despite the very low values in area 1, there is a connection between albitization and Cl enrichment in biotite in that the highest values (taking into account the Mg–Cl avoidance) are in biotite-rich schists. Although the Cl average for biotite from unmetasomatized muscovite schists is 0.21 wt% (Table 3), the high values are from samples of muscovite schist located close to albitite. It is also significant that Cl values up to 0.8% occur in biotite within early-growth andalusite, and that late albite accompanies chlorine-rich biotite in the matrix of some biotite-rich schists. There may thus be a more subtle connection between albitization and Cl enrichment.

TABLE 2. REPRESENTATIVE COMPOSITIONS OF BIOTITE
IN ALBITITES AND BIOTITE-RICH SCHISTS
FROM THE SNAKE CREEK ANTICLINE,
MOUNT ISA INLIER, AUSTRALIA

Sample	404	430.26	430.25	430.4/m	430.4/3	430.4/2	430.4/1	725.3/m	725.3/a
SiO_2 wt%	34.82	37.05	37.99	33.83	33.43	33.82	34.49	34.32	35.40
TiO_2	1.74	2.05	1.58	2.01	2.14	1.95	2.11	1.67	1.95
Al_2O_3	18.44	16.77	17.36	16.94	16.92	17.64	18.21	17.07	17.54
FeO	21.32	14.21	11.76	21.65	22.18	20.59	18.92	21.19	21.73
MnO	b.d.	b.d.	0.28	b.d.	b.d.	b.d.	b.d.	b.d.	b.d.
MgO	7.71	12.04	14.20	7.40	7.31	8.57	9.42	8.06	8.33
CaO	b.d.	b.d.	b.d.	b.d.	b.d.	b.d.	b.d.	b.d.	b.d.
Na_2O	b.d.	b.d.	b.d.	b.d.	b.d.	b.d.	b.d.	b.d.	b.d.
K_2O	9.69	10.37	10.49	9.49	9.64	9.83	10.23	9.27	9.69
Cl	0.17	b.d.	0.60	1.49	1.23	0.30	0.61	0.89	0.33
-O=Cl	0.04	0.00	0.14	0.34	0.28	0.07	0.14	0.20	0.07
Total	93.85	92.49	94.12	92.47	92.57	92.63	93.85	92.27	94.90
Si *apfu*	5.452	5.689	5.667	5.429	5.383	5.381	5.372	5.482	5.493
[IV]Al	2.548	2.311	2.333	2.571	2.617	2.619	2.628	2.518	2.507
[VI]Al	0.855	0.724	0.719	0.471	0.594	0.589	0.715	0.695	0.700
Fe	2.791	1.825	1.467	2.905	0.986	0.739	2.464	2.830	2.819
Mn	0.000	0.000	0.035	0.000	0.000	0.000	0.000	0.000	0.000
Mg	1.800	2.756	3.158	1.771	1.755	2.303	2.187	1.919	1.927
Ti	0.205	0.237	0.178	0.243	0.259	0.233	0.247	0.201	0.228
K	1.935	2.031	1.996	1.943	1.980	1.995	2.032	1.889	1.918
Cl	0.000	0.210	0.152	0.405	0.336	0.081	0.161	0.241	0.087
Total	15.632	15.572	15.704	15.900	15.910	15.770	15.806	15.775	15.678
Mg#	0.39	0.60	0.68	0.38	0.38	0.43	0.47	0.40	0.41

The samples were analyzed at the Advanced Analytical Centre, James Cook University, by energy-dispersion spectrometry using a JXA–840A electron microprobe and Zaph corrections. Minerals and oxides were used as standards. The rock types are as follows: 404: unmetasomatized muscovite–biotite schist, 430.26 and 430.25: albitites, 430.4: biotite-rich schist with andalusite, 725.3: biotite-rich schist with garnet, staurolite and andalusite; m: matrix biotite, 1: biotite in stage-1 andalusite, 2: in stage-2 andalusite, 3: in stage-3 andalusite, a: biotite in andalusite; b.d.: below detection limits. The detection limits for chlorine was generally around 0.14 wt%. The number of atoms, expressed in atoms per formula unit (*apfu*), is based on 22 atoms of oxygen.

TABLE 3. AVERAGE CONCENTRATIONS OF Cl AND
AVERAGE Mg# OF BIOTITE IN ALBITITES
AND BIOTITE-RICH SCHISTS FROM THE SNAKE CREEK ANTICLINE,
MOUNT ISA INLIER, AUSTRALIA

	Muscovite schists	Albitites	Biotite-rich schists	Early andalusite	Late andalusite
wt% Cl	0.21	0.23	0.64	0.20	0.74
Mg#	0.39	0.54	0.49	0.48	0.46

TABLE 4. RANGES AND AVERAGE CONCENTRATION OF Cl
IN BIOTITE FROM THE MATRIX OF MUSCOVITE SCHISTS,
ALBITITES AND BIOTITE-RICH SCHISTS, AND BIOTITE INCLUSIONS
IN ANDALUSITE, SNAKE CREEK ANTICLINE,
MOUNT ISA INLIER, AUSTRALIA

Area of albitization	1	2	3	4–5
Range	b.d.	b.d.–1.37	0.25–1.19	b.d.–0.91
Average	b.d.	0.68	0.64	0.30

Cl concentrations below the limits of detection were treated as zero in the calculations.
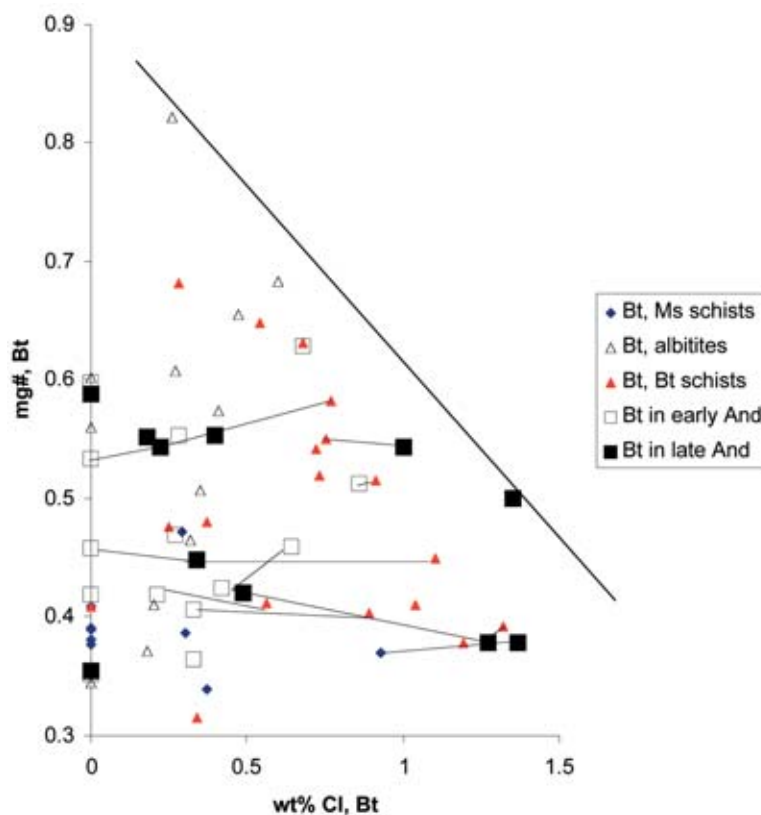
FIG. 9.   Plot of Mg# against wt% Cl for biotite in the matrix and as inclusions in early- and late-stage andalusite. A line indicates the maximum Cl in biotite in rocks from Snake Creek, and reflects Mg–Cl avoidance. Symbols connected with lines indicate, for particular samples, biotite compositions in the matrix and as inclusions in various stages of andalusite growth. Cl values below the theoretical detection-limit (0.14 wt%) are plotted as zero.

The most important reaction to account for the albitization of muscovite schists, muscovite and quartz being replaced by albite, is:

$$KAl_3Si_3O_{10}(OH)_2 + 3Na^+ + 6SiO_2$$
$$= 3NaAlSi_3O_8 + 2H^+ + K^+$$
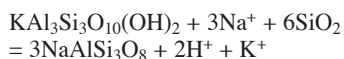
This reaction is based on constant Al, support for which is provided by isocon diagrams plotted for albitites and corresponding schist protoliths (Oliver *et al.*, in press). Note that H$^+$ is released in the reaction, and I contend that Cl enrichment in biotite is connected with HCl that was produced during the albitization reactions. Where the flux of externally derived fluid was high (during peak albitization), only limited interaction occurred with the muscovite schists. The resulting H$^+$ was thus easily diluted and removed from the system. In contrast, dur-

ing periods of low flux, reaction between the schists and NaCl in the fluid was more complete, so that f(HCl)/f(H$_2$O) increased, and biotite became enriched in Cl. Changes during deformation in the activities of Na, K and H due to grain-size reduction and surface ion-exchange (Winsch 1975, Wintsch & Knipe 1983) may have been additional influences on the local equilibria and kinetics of reactions.

Microstructures indicate that albitization and biotite alteration occurred over a protracted period, from D$_1$ to post-D$_3$, and there likely was a significant variation in fluid flux over this period. This model can explain the following points:

1. Based on structural and microstructural observations, albitization peaked during D$_1$, corresponding with the largest changes in Mg# of the biotite. However, albitization continued with less intensity to until after
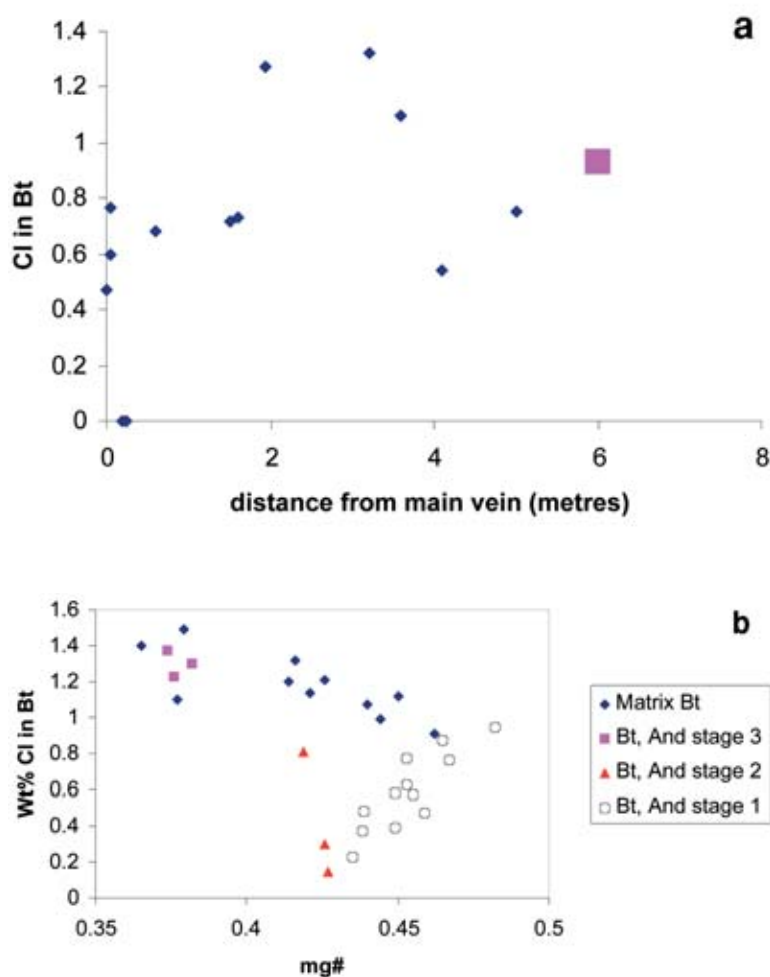
FIG. 10. Plots of composition of matrix biotite against distance from the main albitite at location 430 (Fig. 3). Values for unmetasomatized muscovite schist are plotted for comparison, at an arbitrary distance of 7.5 meters. Symbols are as follows: squares: albitites, diamonds: biotite-rich schists, triangles: unmetasomatized muscovite schists. (a) Mg# for biotite *versus* distance, and (b) wt% Cl in biotite *versus* distance.

the D_3 episode. It was during the waning stages of albitization that build-up of HCl could occur, so that maximum enrichment of Cl in biotite occurred relatively late in the albitization history.

2. The variation in Cl in matrix biotite in the different areas of albitization can be explained in terms of variations in the fluid flux. In area 1, for example, the flux was high during albitization and ceased abruptly, so that no build-up of HCl could take place, resulting in Cl being below detection in biotite in all lithologies.

3. In area 2, the Cl content of biotite in the matrix of albitites and biotite-rich schists was close to the maximum line, except for some shear-zone albitites with over 95% albite, which have very low Cl contents. Since the albitites formed relatively early when the fluid flux was high, the Cl in biotite was initially low and would have remained so in any lithology that was relatively impermeable late in the history, when f(HCl) peaked. The albitites seem to have been relatively impermeable later in the metasomatic history.

4. As a generalization, the Cl content of biotite increased in inclusions in the following order: early andalusite, late andalusite, matrix, most likely owing to increasing f(HCl)/f(H$_2$O) corresponding to waning infiltration of fluid.
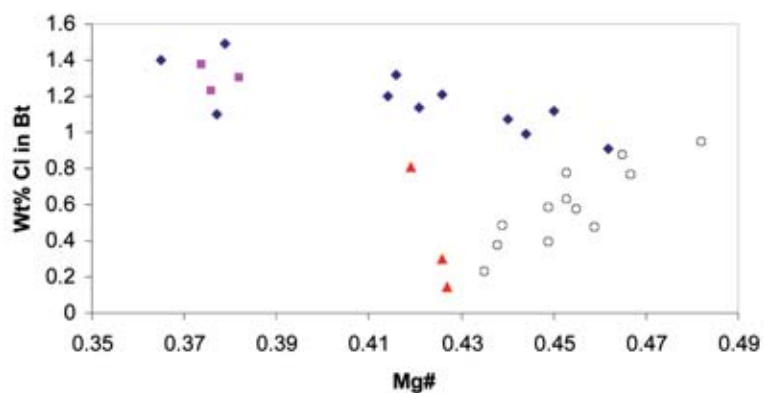
FIG. 11.   Plot of Cl *versus* Mg# for biotite in the matrix and as inclusions in andalusite, sample 430.4 (Figs. 7, 8). Symbols are as follows: diamonds: matrix biotite, squares: biotite inclusions in stage-3 andalusite, triangles: biotite inclusions in stage-2 andalusite, circles: biotite inclusions in stage-1 andalusite.
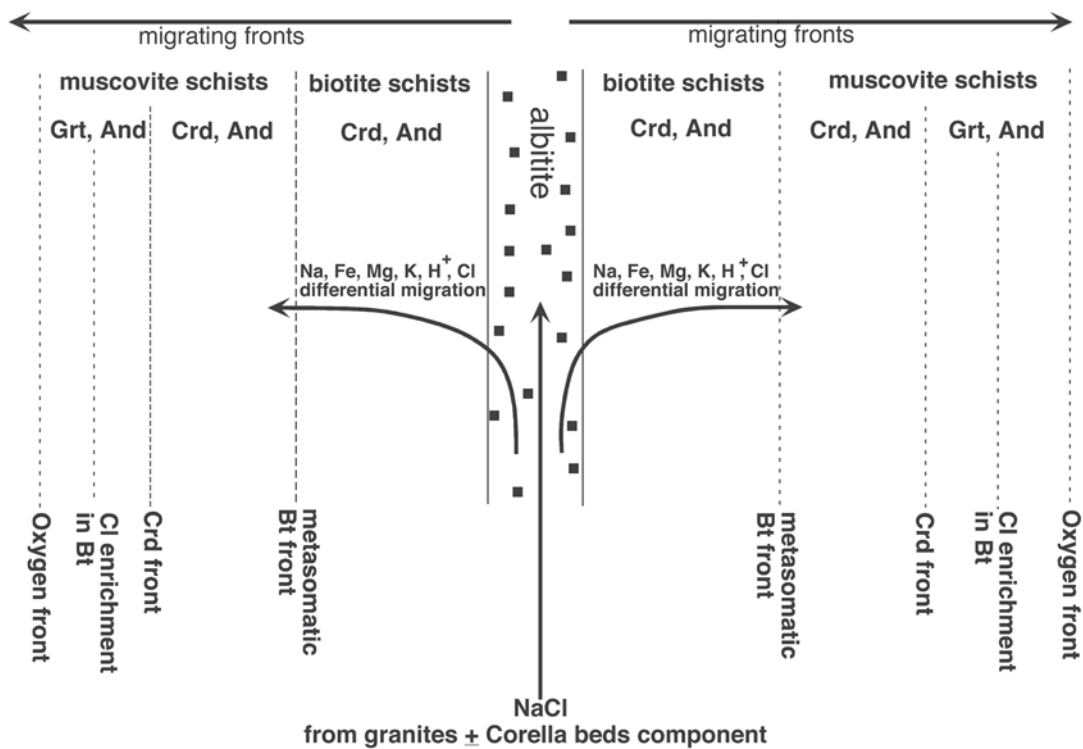

FIG. 12.   Overall model depicting albitization, biotite alteration, and Cl enrichment in biotite. Albitization of schists along shear zones led to depletion of K, Fe, and Mg. Biotite-rich schists formed adjacent to albite-enriched shear-zones by addition of Mg, Na and, in places, Fe. Differential movement of Mg and Fe early in the metamorphic and metasomatic history led to a spatial association of cordierite and albitites. The hydrogen ion, released during the albitization of muscovite, was only allowed to increase during periods of reduced flux of fluid, and led to Cl enrichment in biotite. The oxygen front refers to the limits of resetting of oxygen isotopes by the metasomatizing fluids.

The essential features of the proposed model for albitization and associated alteration and Cl enrichment of biotite are summarized in Figure 12. Infiltration of external fluids was initiated in the D_1 event, producing albitites, in part structurally controlled by shear zones. Iron and Mg were removed during albitization, and, along with Na, were added to adjacent schists to form the biotite-rich metasomatic rocks. Both Fe and Mg moved differentially, so that Mg# varies across the biotite-rich schists. It is uncertain whether any Fe or Mg was also added from the external fluids. The HCl formed as a by-product during the albitization of muscovite, and during the waning stages of albitization (particularly during D_3), $f(HCl)/f(H_2O)$ increased, such that Cl was partitioned into biotite.

Sedimentary rocks in shallow marine and continental margin environments may provide the high-salinity fluids during metamorphism (Yardley & Graham 2002). The source of such fluids is unlikely to be in the host Llewellyn Creek Formation, the original sedimentary rocks being of turbidite origin. However, the Corella beds (or Mary Kathleen Group in general) were originally dolomitic sediments that commonly are evaporitic, as evidenced by the abundance of marialite-rich scapolite (Oliver 1995). Dissolution of evaporites to provide brines was considered by Oliver *et al*. (1994) to explain the widespread occurrence of albitite in the Mary Kathleen Group, but was subsequently rejected as a major source, as stable isotope data suggest equilibration with magmatic fluids (*e.g.,* Oliver *et al*., in press). The Snake Creek albitites have $\delta^{18}O$ values in the range 7.1–10.4‰. For a temperature of albitization of *ca*. 580 C, these values are more consistent with a magmatic origin than brines equilibrated with marble and calc-silicate rocks (M.J. Rubenach, unpubl. data). Another possibility is for essentially magmatic fluids to have contained a component derived from the dissolution of salt-rich beds into the magma prior to its crystallization and to the exsolution of a fluid phase (Oliver *et al*., in press).

ACKNOWLEDGEMENTS

REFERENCES

ADSHEAD, N.D. (1995): *Geology, Alteration and Geochemistry of the Osborne Cu–Au Deposit, Cloncurry District, NW Queensland*. Ph.D. thesis, James Cook Univ., Townsville, Australia.

_____, VOULGARIS, P. & MUSCIO, V.N. (1998): Osborne copper–gold deposit. *In* Geology of Australian and Papua New Guinean Mineral Deposits (D.A. Berkman & D.H. MacKenzie, eds.). *Austral. Inst. Mining Metall.* **222**, 793-799.

BELL, T.H. (1986): Foliation development and refraction in metamorphic rocks: reactivation of earlier foliations and decrenulation due to shifting patterns of deformation partitioning. *J. Metamorph. Geol.* **4**, 421-444.

_____ & HAYWARD, N. (1991): Episodic metamorphic reactions during orogenesis: the control of deformation partitioning on reaction sites and reaction duration. *J. Metamorph. Geol.* **9**, 619-640.

_____ & RUBENACH, M.J. (1983): Sequential porphyroblast growth and crenulation cleavage development during progressive deformation. *Tectonophysics* **92**, 171-194.

BLAKE, D. H. & STEWART, A.J. (1992): Stratigraphic and tectonic framework, Mount Isa Inlier. *In* Detailed Studies of the Mount Isa Inlier (A.J. Stewart & D.H. Blake, eds.). *Aust. Geol. Surv. Org., Bull.* **243**, 1-11.

CARMICHAEL, D.M. (1969): On the mechanisms of prograde metamorphic reactions in quartz-bearing pelitic rocks. *Contrib. Mineral. Petrol.* **20**, 244-267.

DE JONG, G. & WILLIAMS, P.J. (1995): Giant metasomatic system formed during exhumation of mid-crustal Proterozoic rocks in the vicinity of the Cloncurry Fault, northwest Queensland. *Aust. J. Earth Sci.* **42**, 281-290.

FOSTER, D. & RUBENACH, M.J. (2001): High radiogenic heat-producing granites and metamorphism – an example from the western Mount Isa Inlier, Australia: comment. *Geology* **28**, 671.

GAUTIER, L., HALL, G., STEIN, H. & SCHALTEGGER, U. (2001): The Osborne Deposit, Cloncurry District: a 1595 Ma Cu–Au skarn deposit. *In* A Hydrothermal Odyssey (P.J. Williams, ed.). *Economic Geology Research Unit, Contrib.* **59**, 58-59 (abstr.).

GILES, D. & NUTMAN A.P. (2002): SHRIMP U–Pb monazite dating of 1600–1580 Ma amphibolite facies metamorphism in the southeastern Mt Isa Block, Australia. *Aust. J. Earth Sci.* **49**, 455-465.

GOLEBY, B.R., DRUMMOND, B., MACCREADY, T. & GONCHAROV, A. (1996): The Mount Isa deep seismic transect. *In* MIC'96, New Developments in Metallogenic Research: the McArthur, Mount Isa, Cloncurry Mineral Province (T. Baker, J.F. Rotherham, G. Mark & P.J. Williams, eds.). *James Cook University Economic Geology Research Unit, Contrib.* **55**, 51-55.

KRETZ, R. (1983): Symbols for rock-forming minerals. *Am. Mineral.* **68**, 277-279.

LOOSVELD, R.J.H. (1989): The synchronism of crustal thickening and high T/low P metamorphism in the Mount Isa Inlier, Australia. 1. An example, the central Soldiers Cap Group. *Tectonophysics* **158**, 173-190.

MARK, G., DARVALL, M. , TOLMAN, J., FOSTER, G.R.W., WILLIAMS, P.J. & POLLARD, P.J. (1999): Magmas and regional Na–Ca alteration, Cloncurry district, Australia. *In* Mineral Deposits: Processes to Processing (C.J. Stanley *et al.*, eds.). Balkema, Rotterdam, The Netherlands (385-388).

_____, PHILLIPS, G.N. & POLLARD, P.J. (1998): Highly selective partial melting of pelitic gneiss at Cannington, Cloncurry district, Queensland. *Aust. J. Earth Sci.* **45**, 169-175.

MCLELLAND, J., MORRISON, J., SELLECK, B., CUNNINGHAM, B., OLSON, C. & SCHMIDT, K. (2002): Hydrothermal alteration of late- to post-tectonic Lyon Mountain Granitic Gneiss, Adirondack Mountains, New York: origin of quartz–sillimanite segregations, quartz–albite lithologies, and associated Kiruna-type low-Ti Fe-oxide deposits. *J. Metamorph. Geol.* **20**, 175-190.

MUNOZ, J.L. (1984): F–OH and Cl–OH exchange in micas with applications to hydrothermal ore deposits. *In* Micas (S.W. Bailey, ed.). *Rev. Mineral.* **13**, 469-494.

_____ (1992): Calculation of HF and HCl fugacities from biotite compositions: revised equations. *Geol. Soc. Am., Abstr. Programs* **24**, A221.

_____ & SWENSON, A. (1981): Chloride–hydroxyl exchange in biotite and estimation of relative HCl/HF activities in hydrothermal fluids. *Econ. Geol.* **76**, 2212-2221.

OLIVER, N.H.S. (1995): Hydrothermal history of the Mary Kathleen Fold Belt, Mt Isa Block, Queensland. *Aust. J. Earth Sci.* **42**, 267-280.

_____, CARTWRIGHT, I., WALL, V.J. & GOLDING, S.D. (1993): The stable isotope signature of kilometre-scale fracture-dominated metamorphic fluid pathways, Mary Kathleen, Australia. *J. Metamorph. Geol.* **11**, 705-720.

_____, MARK, G., CLEVERLY, J., POLLARD, P.J., FU, BIN, MARSHALL, L.J., WILLIAMS, P.J. & BAKER, T. (2004): The role of sodic alteration in the genesis of iron oxide – copper – gold deposits, eastern Mt Isa Block, Australia. *Econ. Geol.* **99**, 1145-1176.

_____, RAWLING, T.J., CARTWRIGHT, I. & PEARSON, P.J. (1994): High temperature fluid–rock interaction and scapolitization in a large extension-related hydrothermal system, Mary Kathleen, Australia. *J. Petrol.* **35**, 1455-1491.

_____, WALL, V.J. & CARTWRIGHT, I. (1992): Internal controls of fluid compositions in amphibolite-facies scapolitic calc-silicates, Mary Kathleen, Australia. *Contrib. Mineral. Petrol.* **111**, 94-112.

PAGE, R.W. & SUN, S.-S. (1998): Aspects of geochronology and crustal evolution in the Eastern Fold Belt, Mount Isa Inlier. *Aust. J. Earth Sci.* **45**, 343-361.

REINHARDT, J. & RUBENACH, M.J. (1989): Temperature–time relationships across metamorphic zones: evidence from porphyroblast–matrix relationships in progressively deformed metapelites. *Tectonophysics* **158**, 141-161.

RUBENACH, M.J., ADSHEAD, N.D., OLIVER, N.H.S., TULLEMANS, F., ESSER, D. & STEIN, H. (2001): The Osborne Cu–Au deposit: geochronology and genesis of mineralization in relation to host albitite and ironstones. *In* A Hydrothermal Odyssey (P.J. Williams, ed.). *Economic Geology Research Unit, Contrib.* **59**, 172-173 (abstr.).

_____ & BARKER, A.J. (1998): Metamorphic and metasomatic evolution of the Snake Creek Anticline, Eastern Succession, Mount Isa Inlier. *Aust. J. Earth Sci.* **45**, 363-372.

_____ & LEWTHWAITE, K.A. (2002): Metasomatic albitites and related biotite-rich schists from a low-pressure polymetamorphic terrane, Snake Creek Anticline, Mount Isa Inlier, north-eastern Australia: microstructures and P–T–t paths. *J. Metamorph. Geol.* **20**, 191-202.

VERNON, R.H. (1978): Porphyroblast–matrix microstructural relationships in deformed metamorphic rocks. *Geol. Rundsch.* **67**, 288-305.

_____ (1979): Formation of late sillimanite by hydrogen metasomatism (base-leaching) in some high-grade gneisses. *Lithos* **12**, 143-152.

WILLIAMS, P.J. (1998): Metalliferous economic geology of the Mt Isa Eastern Succession, Queensland. *Aust. J. Earth Sci.* **45**, 329-341.

_____, DONG, GUOYI, POLLARD, P.J., PERRING, C.S., RYAN, C.G. & MERNAGH, T.P. (1999): Fluid inclusion geochemistry of Cloncurry (Fe)–Cu–Au deposits. *In* Mineral Deposits: Processes to Processing (C.J. Stanley, ed.). Balkema, Rotterdam, The Netherlands (111-114).

WINTSCH, R.P. (1975): Feldspathization as a result of deformation. *Geol. Soc. Am., Bull.* **86**, 35-38.

_____ & KNIPE, R.J. (1983): Growth of a zoned plagioclase porphyroblast in a mylonite. *Geology* **11**, 360-363.

YARDLEY, B.W.D. & GRAHAM, J.T. (2002): The origins of salinity in metamorphic fluids. *Geofluids* **2**, 249-256.

ZHU, CHEN & SVERJENSKY, D.A. (1991): Partitioning of F–Cl–OH between minerals and hydrothermal fluids. *Geochim. Cosmochim. Acta* **55**, 1837-1858.

ZWART, H.J. (1960): Relations between folding and metamorphism in the central Pyrenees, and their chronological succession. *Geol. Mijnbouw* **39**, 163-180.